UNIVERSITY OF LEEDS

This is a repository copy of *Engineering of light confinement in strongly scattering disordered media*.

White Rose Research Online URL for this paper:
http://eprints.whiterose.ac.uk/89269/

Version: Accepted Version

Engineering of light confinement in strongly scattering disordered media.

Francesco Riboli[1,2,a,*], Niccolò Caselli[1,2], Silvia Vignolini[1,2,b], Francesca Intonti[1,2], Kevin Vynck[1,c], Pierre Barthelemy[1,d], Annamaria Gerardino[3], Laurent Balet[4], Lianhe H. Li[4], Andrea Fiore[4,e], Massimo Gurioli[1,2] and Diederik S. Wiersma[1,2].

[1] European Laboratory for Non-linear Spectroscopy, Via N. Carrara 1 50019 Sesto Fiorentino (FI), Italy

[2] Department of Physics, University of Florence, Via G. Sansone 1, 50019 Sesto Fiorentino (FI), Italy

[3] Institute of Photonics and Nanotechnology, CNR, Via C. Romano 42, 00156 Roma, Italy

[4] Ecole Polytechnique Fédérale de Lausanne, Institute of Photonics and Quantum Electronics, CH-1015 Lausanne, Switzerland

*email: f.riboli@unitn.it

Present address:

[a] Department of Physics, University of Trento, via Sommarive 14, 38123 Povo (TN), Italy

[b] Melville Laboratory for Polymer Synthesis, Department of Chemistry, University of Cambridge, Lensfield Road, Cambridge CB2 1EW, United Kingdom.

[c] Laboratoire Photonique, Numérique et Nanosciences (LP2N), UMR 5298, CNRS - IOGS - Université Bordeaux, Institut d'Optique d'Aquitaine, 33400 Talence, France

[d] Quantum Transport, Kavli Institute of Nanoscience, TU Delft, Lorentzweg 1,2628 CJ Delft,The Netherlands

[e] COBRA Research Institute, Eindhoven University of Technology, 5600 MB Eindhoven, The Netherlands

Disordered photonic materials can diffuse and localize light through random multiple scattering, offering opportunities to study mesoscopic phenomena, control light-matter interaction, and provide new strategies for photonic applications. Light transport in such media is governed by photonic modes characterized by resonances with finite spectral width and spatial extent. Considerable steps have been made recently towards the control over transport using wavefront shaping techniques. The selective engineering of individual modes, however, has only been addressed theoretically. Here, we experimentally demonstrate the possibility to engineer the

confinement and the mutual interaction of modes in a two-dimensional disordered photonic structure. The strong light confinement is achieved at the fabrication stage by an optimization of the structure and an accurate and local tuning of the modes resonance frequency is achieved via post-fabrication processes. To show the versatility of our technique, we selectively control the detuning between overlapping localized modes and observe both frequency crossing and anti-crossing behaviours, thereby paving the way for the creation of open transmission channels in strongly scattering media.

The ability to mold the flow of light at the wavelength scale has been largely investigated in photonic-crystal-based devices, a class of materials in which the propagation of light is driven by interferences between multiply Bragg scattered waves and whose energy dispersion is described by a photonic band diagram [1]. Light propagation in such structures is defined by Bloch modes, which can be engineered by varying the structural parameters of the material [2-4]. In disordered media, both the direction and phase of the propagating waves are randomized in a complex manner, making any attempt to control light propagation particularly challenging. Disordered media are currently investigated in several contexts, ranging from the study of collective multiple scattering phenomena [5,6] to cavity quantum electrodynamics and random lasing [7,8], to the possibility to provide efficient solutions in renewable energy [9], imaging [10], and spectroscopy-based applications [11]. Transport in such systems can be described in terms of photonic modes, or quasi-modes, which exhibit characteristic spatial profiles and spectra [12,13]. In diffusive systems, these modes are spatially and spectrally overlapping while in the regime of Anderson localization, they become spatially and spectrally-isolated [14]. Unlike Bloch modes in periodic systems, the precise formation of photonic modes in a single realization of the disorder is unpredictable. Control over light transport can be obtained by shaping the incident wave to excite only a specific part of the modes available in a given system [15-18]. For fully exploiting the potential of disordered systems, however, a mode control is needed. It was shown

theoretically that isolated modes could be selectively tuned and possibly coupled to each other by a local fine modification of the dielectric structure [19,20].

In this Article, we demonstrate experimentally the ability to fully control the spectral properties of an individual photonic mode in a two-dimensional disordered photonic structure [21], in a wavelength range that is relevant for photonic research driven applications. A statistical analysis of individual spatially-isolated random photonic modes is performed by multi-dimensional near-field imaging, leading to a detailed determination of intensity fluctuations, decay lengths and mode volumes. We then demonstrate that individual modes can be fine-tuned either by near-field tip perturbation or by local sub-micrometer-scale oxidation of the semiconductor slab [22]. The resonant frequency of a selected mode is gradually shifted until it is in perfect spectral superposition with the frequency of other two modes, located a few micrometers apart and spatially overlapping with the tuned mode. On spectral resonance, we observe frequency crossing and anti-crossing behaviours, respectively, the latter indicating mode interaction. This provides the experimental proof-of-principle that optically isolated regions can be connected [23], offering new possibilities in the control of light propagation in disordered media.

The samples under consideration are 320nm thick GaAs planar dielectric waveguides, optically activated by the inclusion of three layers of In-As quantum dots (QDs) at the center of the slab and patterned with disordered distributions of circular holes with varying parameters, see the SEM images in Figures 1 (a) and (b). The system is studied by using a commercial Near Field Scanning Optical Microscope (SNOM), used in illumination/collection geometry at room temperature. Further experimental details on the sample design, fabrication and near field imaging are given in the Methods section.

Figures 1 (c) and (d) show typical Photo-Luminescence (PL) near-field intensity maps at fixed emission wavelength for samples with f=0.35 and f=0.13 respectively (f is the filling fraction, defined as the ratio between the area occupied by the scatterers and the total area of the sample). Several modes, with a high degree of spatial localization, are identified by the bright spots in the intensity distributions and peaks in the wavelength spectrum (the spectra

corresponding to the highest intensity spots in Figures 1 (c) and (d) are shown in Figures 1 (e) and (f), respectively). The main difference between the two spectra normalized to the average intensity is the peak amplitude value. In fact, the PL spectrum of the sample with f=0.35 supports a peak 10 times more intense than the average value, while the PL spectrum of the sample with f=0.13 exhibits a peak with an intensity 3.5 times the average value. While such intensity distributions and spectra provide useful local information about two single peaks, a statistical analysis of a large dataset is required to understand the mesoscopic properties of individual samples, and in particular the influence of the hole filling fraction and diameter to the properties of the underlying modes.

Figures 2 (a) and (b) show the Probability Density Function (PDF) of the near-field PL intensity normalized to the PL average value (I_{PL}/<I_{PL}>). Each distribution has been evaluated taking into account all intensity maps within the experimental spectral range (between λ=1.15 μm and λ=1.38 μm). Increasing the filling fraction leads to more asymmetric (Fig. 2 (a)) and heavy-tailed (Fig. 2 (b)) PDFs with notably a higher probability to observe high intensity peaks. For instance, peaks with a normalized intensity of about I_{PL}/<I_{PL}>=4 are about 100 times more probable in samples with f=0.35 that in those with f=0.2. The onset of the occurrence of rare yet very bright peaks can be quantified by the normalized variance σ^2/μ^2 of the PDF (where σ^2 and μ are the variance and the mean intensity of the distribution, respectively). Figure 2 (c) shows that σ^2/μ^2 increases by at least a factor of five by increasing the filling fraction from f=0.13 to f=0.35. The influence of the hole diameter (h_d) on the normalized variance is less evident as shown by the three behaviours of σ^2/μ^2 highlighted with squares, circles and triangles that correspond to h_d=180nm, h_d=200nm, h_d=250nm, respectively. The PL fluctuations of the integrated quantum sources are primarily driven by the Local Density of States (LDOS) fluctuations [24,25], which in turn are related to the light transport properties of the system but also to the near-field interaction between sources and scatterers [26-28]. In our experimental configuration the interplay between the involved processes, like the excitation efficiency of QDs, the collection efficiency

of the SNOM tip and the light transport in the disordered medium, does not allow to quantitatively relate the slopes of the PDF tails with the dimensionless conductance [24,29,30] and to quantify the contribution of the light transport properties and source-scatterer near-field interaction to such fluctuations. Nevertheless, the appearance of longer tails for samples with increasing filling fraction is a signature of the increased confinement of the photonic quasi-modes. On the other hand, the weak dependence of the fluctuations on the hole diameter shows that such disordered systems are structurally independent (within the measurement spectral window), to possible scatterer size-dispersion.

To retrieve information onto the average spatial extension of the photonic modes, we exploit the fact that their quality factor should decrease in proximity to the sample borders due to in-plane leakage. Basically, the more confined modes will feel the sample borders at shorter distances from it. The average mode decay length may then be evaluated by investigating how the mode spectral width depends on distance to the border [31]. Figures 3 (a) and (b) show the full width at half maximum (FWHM) of the averaged frequency autocorrelation function of the near-field spectra, collected in spatial strips parallel to the sample border as a function of distance to the border. The average FWHM decreases very rapidly for samples with f=0.35 (h_d=200 nm), reaching a constant value at a distance of 3-4 μm away from the border, while for samples with f=0.13 (h_d=200 nm) the decay is much slower, reaching a constant value at a distance of about 10-12 μm. Figure 3 (c) shows the decay length, as calculated from an exponential fit to the FWHM decrease with distance to the border, as a function of the density of scatterers. The samples with f=0.35 supports modes with decay length of about ξ=0.8 μm with a ratio (L/2)/ξ=15, where L=25 μm is the sample size, while for f=0.13 the decay length is about ξ=3.5 μm with a ratio (L/2)/ξ=3.5. The FWHM of frequency autocorrelations in the middle of the samples is related to the spectral width of localized modes, that provide their average intrinsic quality factor Q =λ_0/$\delta\lambda$=440+/-80 for f=0.35 (h_d=200 nm). This value is bounded by the out-of-plane losses that are roughly four times

larger than the in-plane losses (inherent to the finite size of the sample), as we have verified by the comparison between 2D and 3D FDTD calculations.

Having identified a proper set of design parameters to create disordered structures that support strongly confined modes, we proceed to a post-processing step that allows fine-tuning the resonant wavelength of such modes. The technique we exploit is based on the local modification of the dielectric environment in the proximity of the maximum intensity of the modes. From a sample in the regime of the strongest confinement, at f=0.35 and h_d=200nm, we demonstrate the ability to (i) perform a gentle and reversible spectral tuning on a single localized mode and to (ii) engineer the wavelength splittings of selected pairs of modes that show a crossing or an anti-crossing feature, depending on the mutual spatial overlap and therefore on the mode interaction strength [32].

The gentle and reversible engineering is achieved by exploiting the perturbation induced by the SNOM tip, which modifies the local dielectric environment where multiple light scattering takes place [31]. For a dielectric uncoated SNOM tip, the induced spectral shift is towards lower energies and the amplitude given by $\Delta\lambda/\lambda_0=(\lambda_{max}-\lambda_0)/\lambda_0$ is proportional to the modal volume V_{eff} of the localized mode and to the SNOM tip polarizability [33,34]. Figure 4 (a) shows the intensity image of an isolated mode that extends over a region of a few micrometers, while Figure 4 (b) shows the normalized intensity spectra taken close to the PL maximum intensity of the mode (point A) and on the PL low intensity tail (point B). The amplitude of the observed spectral shift is $\Delta\lambda$=(0.43+/-0.02) nm, which represents a small fraction of the mode linewidth ($\delta\lambda$~3 nm), but demonstrates that a dielectric perturbation in the near-field is able to slightly modify the resonant frequency of a disordered mode. This spectral shift allows also to give an estimation of the modal volume of the localized mode V_{eff}~0.2 μm^3 [35], a value consistent both with the SNOM mode image (Fig. 4 (a)) and with the statistical estimation of the decay length (Fig. 3 (c)).

In order to control the modes in a broader spectral range, we exploit the post-fabrication technique based on a laser assisted micro-oxidation that permanently and locally (~1μm^2)

modifies the dielectric environment by reducing the effective GaAs membrane thickness and by increasing the effective pore diameter [22]. This technique has been successfully used to gently blue-shift the resonance frequency of photonic-crystal-based cavities and has also been theoretically proposed as a way to change the nature of the modes in a strongly disordered system [19]. We carefully choose a set of three modes that are spatially close but detuned in frequency to demonstrate the ability to engineer the spectral and spatial properties of the modes.

Figures 5 (a), (b) and (c) show the intensity PL distribution of the three modes (mode A, mode B and mode C) before starting the laser assisted oxidation process. The PL distribution of each mode is characterized by a main intensity peak surrounded by speckles with lower intensities. The spatial regions highlighted by the white (red) dotted lines, identify the spatial overlap between the A and B (B and C) modes. The laser exposition is made in correspondence to the maximum intensity of mode B (white circle). Figures 5 (e) and (g) show the temporal evolution as a function of the laser exposure time of the normalized PL spectra averaged over the BC and AB overlap regions, respectively. The lower PL intensity in BC with respect to AB (demonstrated by the larger signal to noise ratio in the normalized spectra) reflects the smaller spatial overlap between the modes. Figure 5 (f) shows the evolution of the resonant wavelengths of modes A, B and C as a function of the laser exposure time Δt. Let us first consider the time evolution of the mode B respect to the mode C. The wavelength of mode B (λ_B) blue-shifts monotonically while that of mode C (λ_C) stays at the unperturbed value within the experimental uncertainty. After 310 minutes of exposure, the spectral overlap between the two modes is maximized. By further oxidizing the dielectric membrane, the two resonances spectrally cross until they go out of resonance at $\Delta t=465$ minutes. The spatial overlap between modes B and C is quite small, thus determining a coupling strength much smaller than the broadening of the individual modes [19]. The two modes are likely to be in the weak coupling regime, explaining why a frequency anti-crossing is not observed. One possible way to get greater interaction strength is to choose two modes

with a larger spatial overlap, which means a shorter spatial separation. This is exactly the case of mode A and mode B, which have a larger spatial overlap respect to the previous case (BC). The time evolution of the A and B wavelengths reported in Figure 5 (f) shows that the local oxidation induces mode anti-crossing. Indeed, the splitting between the mode resonant wavelengths as a function of the exposure time ($\Omega_{AB}=\lambda_A-\lambda_B$) initially decreases, reaching the minimum around $\Delta t=170$ min and then increasing again (see panel (d)).The amplitudes of the two interacting modes in the overlap region reach the same value at the time of minimum splitting (see the evolution of the PL spectra in panel (g)). The black solid line in panel (d) is the result of the fit of the experimental splitting with the expected strong coupling behaviour [36]. The minimum experimental splitting Ω^0_{AB}, gives the interaction strength g by $\Omega^0_{AB}=2g=(3.55+/-0.25)$ nm. To satisfy the strong coupling condition, Ω^0_{AB} has to be compared with the FWHM of the modes that is $\Delta\lambda=(3.00+/-0.08)$ nm; we find that $\Omega^0_{AB} \geq \Delta\lambda$ that means that the two modes are just at the onset of strong coupling. Our observation of both frequency crossing and anti-crossing behaviours represents the first step towards the creation of chains of hybridized localized random modes, better known as necklace states, observed in 1D-systems [37] and predicted for higher dimensions [23].

In conclusion, we have shown that it is possible to obtain and engineer strongly confined modes in two-dimensional disordered structures in the near-infrared wavelength regime. More strikingly, we have demonstrated the possibility to largely engineer the spectrum and the interaction of random modes by a fine-tuning of the disordered system in post-fabrication processes. Our results open new routes for addressing mesoscopic transport phenomena in random media. As an example, the control of the optical confinement and of the coupling between modes could be used to exploit 2D necklace states for designing transmission channels. In addition, random photonic materials have been proposed as an alternative platform to develop both classical and quantum photonic devices, and, in this framework, our achievements constitute an important step towards the control of disorder-based photonic resonators and traps.

Author contributions

FR designed and engineered the samples. MG conceived the post fabrication tuning of random modes. NC, FI, FR and SV performed the experiments. FR and NC performed the data analysis with help from MG, KV, FI, PB and DSW. AG, LL, LB and AF fabricated the samples. FR and MG wrote the paper with support from KV, FI, NC and with appraisals and inputs from DSW. FR, KV, PB, DSW and MG contributed to the theoretical analysis. All authors contributed to the general discussion.

References

[1] Joannopoulos, J. D., Johnson, S. G., Winn, J. N. & Meade, R. D. *Molding the Flow of Light* 2nd edn. (Princeton University Press 2008).

[2] Akahane, Y., Asano, T., Song, B. S. & Noda, S. High-Q photonic nanocavity in a two-dimensional photonic crystal. *Nature* **425,** 944-947, (2003).

[3] Yanik, M. F. & Fan, S., Stopping light all optically. *Phys. Rev. Lett.* **92,** 083901, (2004).

[4] Tran, N. V., Combrié, S. & De Rossi, A. Directive emission from high-Q photonic crystal cavities through band folding. *Phys. Rev. B.* **79,** 041101(R), (2009).

[5] Strudley, T., Zehender, T., Blejean, C., Bakkers, E. P. A. M. & Muskens, O. Mesoscopic light transport by very strong collective multiple scattering in nanowire mats. *Nature Photon.* **7,** 413 (2013).

[6] Payne, B., Yamilov, A. & Skipetrov, S. E. Anderson localization as position-dependent diffusion in disordered waveguides. *Phys. Rev B.* **82,** 024205 (2010).

[7] Sapienza, L. *et al.* Cavity quantum electrodynamics with Anderson-localized modes. *Science* **327,** 1352-1355 (2010).

[8] Noh, H. *et al.* Control of lasing in biomimetic structures with short range order. *Phys. Rev Lett..* **106,** 183901 (2011).

[9] Vynck, K., Burresi, M., Riboli, F. & Wiersma, D. S. Photon management in two-dimensional disordered media. *Nature Mater.* **11,** 1017-1022 (2012).

[10] Bertolotti, J. *et al.* Non-invasive imaging through opaque scattering layers. *Nature* **491,** 232-234 (2012).

[11] Redding, B., Liew, S., F., Sarma, R. and Cao, H. Compact spectrometer based on a disordered photonic chip. *Nature Photon.* **7,** 746 (2013).

[12] Sheng, P. *Introduction to Wave Scattering, Localization and Mesoscopic Phenomena* 2nd edn. (Springer 2010).

[13] Ching, E. S. C. et al. Quasinormal-mode expansion for waves in open systems. *Rev. Mod. Phys.* **70,** 1545-1554 (1998).

[14] A. Z. Genack and S. Zhang, "Wave interference and modes in random media", Chapter 9 in *Tutorials in Complex Photonic Media*, eds. M. A. Noginov et al. (SPIE Publications, 2009).

[15] Popov, S., M. *et al.* Measuring the Transmission Matrix in Optics: An Approach to the Study and Control of Light Propagation in Disordered Media. *Phys. Rev. Lett.* **104,** 100601 (2010).

[16] Mosk, A., Lagendijk, A., Lerosey, G. & Fink, M. Controlling waves in space and time for imaging and focusing in complex media. *Nature Photon.* **6,** 283 (2012).

[17] Leonetti, M., Conti, C. & Lopez, C. Switching and amplification in disordered lasing resonators. *Nature Commun.* **4,** 1740 (2013).

[18] Bachelard, B., Andreasen, J., Gigan, S. & Sebbah, P. Taming random lasers through active spatial control of the pump. *Phys. Rev. Lett.* **109,** 033903 (2012).

[19] Labonté, L. Vanneste, C. & Sebbah, P. Localized mode hybridization by fine tuning of two-dimensional random media. *Opt. Lett.* **37,** 1946-1948 (2012).

[20] Vanneste, C. & Sebbah, P. Complexity of two-dimensional quasimodes at the transition from weak scattering to Anderson localization. *Phys. Rev. A.* **79,** 041802(R) (2009).

[21] Riboli, F. *et al.* Anderson localization of near-visible light in two dimensions. *Opt. Lett.* **36,** 127-129 (2011).

[22] Intonti, F. *et al.* Mode tuning of photonic crystal nanocavities by photoinduced non-thermal oxidation. *Appl. Phys. Lett.* **100,** 033116 (2012).

[23] Pendry, J. B. Quasi-extended electron states in strongly disordered systems. *J. Phys. C* **20,** 733 (1987).

[24] Mirlin, A. D., Statistic of energy levels and eigenfunctions in disordered systems. *Phys. Rep.* **326,** 259 (2000).

[25] van Tiggelen, B., A. & Skipetrov, S., E. Fluctuations of local density of states and C_0 speckle correlations are equal. *Phys. Rev. E* **73,** 045601(R), (2006).

[26] Cazé, A., Pierrat, R. & Carminati, R. Near-field interactions and nonuniversality in speckle patterns produced by a point source in a disordered medium, *Phys. Rev. A* **82,** 043823 (2010).

[27] Sapienza, R. *et al.* Long-tail statistics of the Purcell factor in disordered media by near field interaction. *Phys. Rev. Lett.* **106,** 163902 (2011).

[28] Birowosuto, M. D., Skipetrov, S. E. Vos, W. L. & Mosk, A. P. Observation of spatial fluctuations of the local density of states in random photonic media. *Phys. Rev. Lett.* **105,** 013904 (2010).

[29] Garcia, P. D., Stobbe, S., Sollner, I. & Lodahl, P. Nonuniversality intensity correlations in a two-dimensional Anderson-localizing random medium. *Phys. Rev. Lett.* **109,** 253902 (2012).

[30] Nieuwenhuizen, Th. M. & van Rossum, M. C. W. Intensity distributions of waves transmitted through a multiple scattering medium. *Phys. Rev. Lett.* **74,** 2674–2677 (1995).

[31] Laurent, D., Legrand, O., Sebbah, P.,Vanneste, C. & Mortessagne, F. Localized modes in a finite-size open disordered microwave cavity. *Phys. Rev. Lett.* **99,** 253902 (2007).

[32] Berman, P. R. (ed.) *Cavity Quantum Electrodynamics* (Academic, Boston, 1994).

[33] Koenderink, A., F., Kafesaki, M., Buchker, B., C. & Sandoghdar, V. Controlling the resonance of a photonic crystal microcavity by near-field probe. *Phys. Rev. Lett.* **95,** 153904 (2005).

[34] Intonti, F. *et al.* Spectral tuning and near-field imaging of photonic crystal microcavities. *Phys. Rev. B*, **78,** 041401(R), (2008).

[35] Spasenovic, M., Beggs, D., M., Lalanne, P., Krauss, T., F. & Kuipers, L. Measuring the spatial extent of individual localized photonic states. *Phys. Rev. B*, **86,** 155153 (2012).

[36] Intonti, F. et al. Nanofluidic control of coupled photonic crystal resonator. *Appl. Phys. Lett.* **96,** 141114, (2010).

[37] Bertolotti, J., Gottardo, S., Wiersma, D. S., Ghulinyan, M., Pavesi, L. Optical necklace states in Anderson localized 1D systems. *Phys. Rev. Lett.* **94,** 113903 (2005).
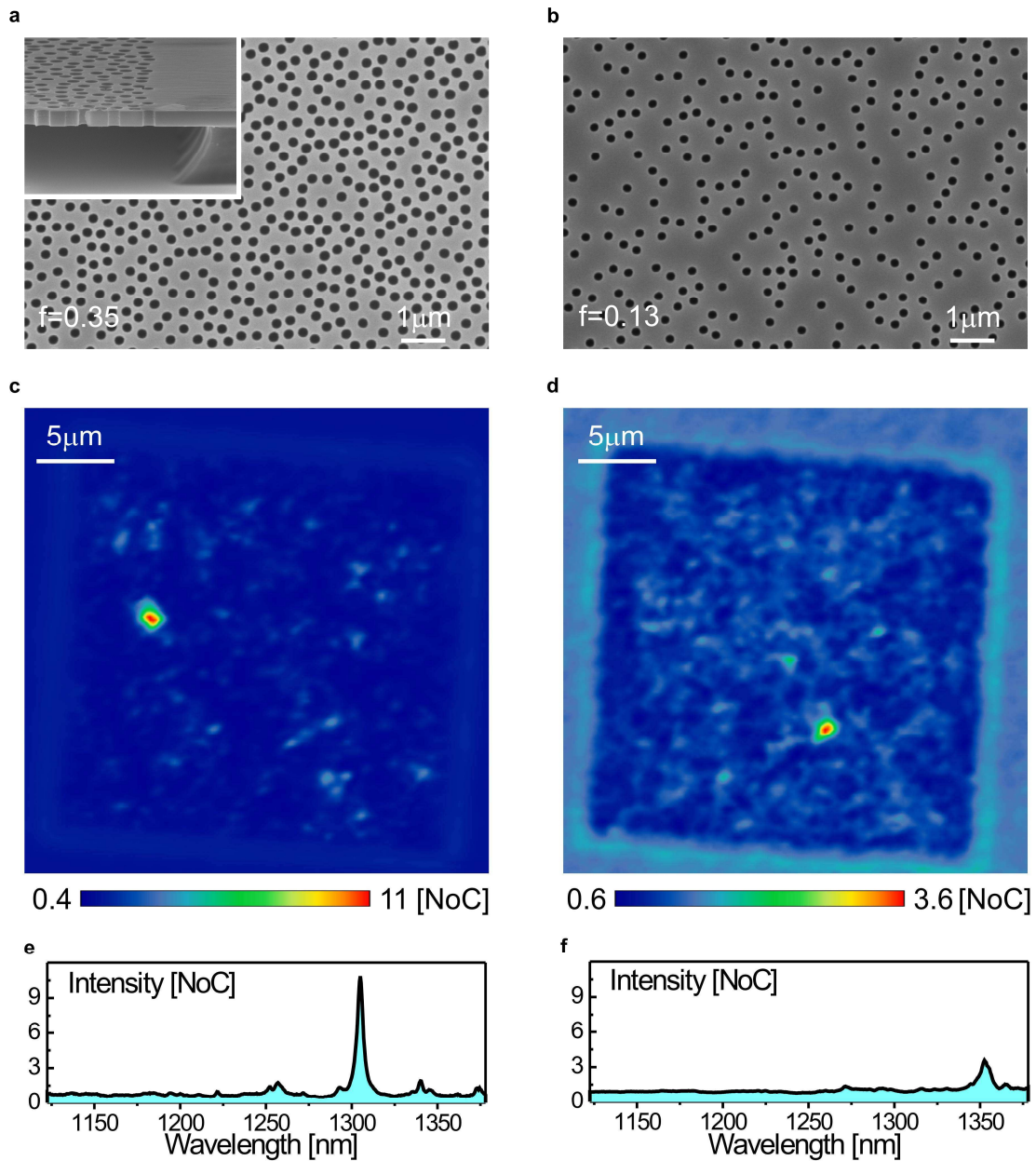
FIGURE 1: **Near field imaging of localized modes. a-b,** Scanning Electron Microscopy (SEM) images of disordered samples with f=0.35 and f=0.13 and hole diameters h_d=215 nm and h_d=185 nm, respectively. The inset of panel (**a**) shows the suspended photonic membrane clamped at its edges. **c-d,** Near field photo-luminescence images for samples with f=0.35 and f=0.13, at the wavelength of the main peak of the near-field spectra reported in (**e**) and (**f**) respectively. The near-field spectra have been picked up in correspondence of the most intense spatially-localized peak and normalized to the average photoluminescence of the whole sample. The color scale of the near-field images and the vertical scale in the

wavelength spectra range from the minimum to the maximum of the Normalized number of counts [NoC].
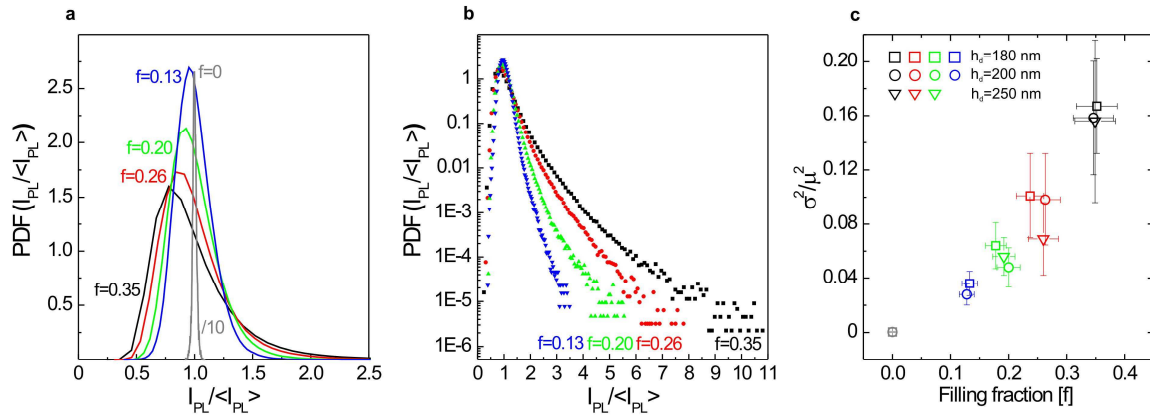

FIGURE 2: **Statistical distributions of the PL intensity. a-b,** Probability Density Function of the near-field intensities for different values of the filling fraction ($f=0$, $f=0.13$, $f=0.2$, $f=0.26$, $f=0.35$) and $h_d=200$ nm. Each curve has been evaluated taking into account 512 near-field intensities maps within the wavelength range 1.15 μm - 1.37 μm. Each map is composed by 10^4 pixels. The PL intensities (I_{PL}) are normalized to the PL average value of the photoluminescence of the respective sample ($\mu=<I_{PL}>$). The linear scale (**a**), shows also the distribution for $f=0$ (divided by a factor of 10), i.e. the slab without any holes, exhibiting the minor fluctuations due to the In-Ga-As quantum dots themselves. **c,** Variance (σ^2) of PDFs for different scatterers diameter, normalized to the average value μ. The error bar of σ^2/μ^2 has been evaluated by calculating this quantity for different ranges of wavelengths, while for the filling fractions the uncertainty comes from the dispersion of the hole diameters evaluated with SEM images.
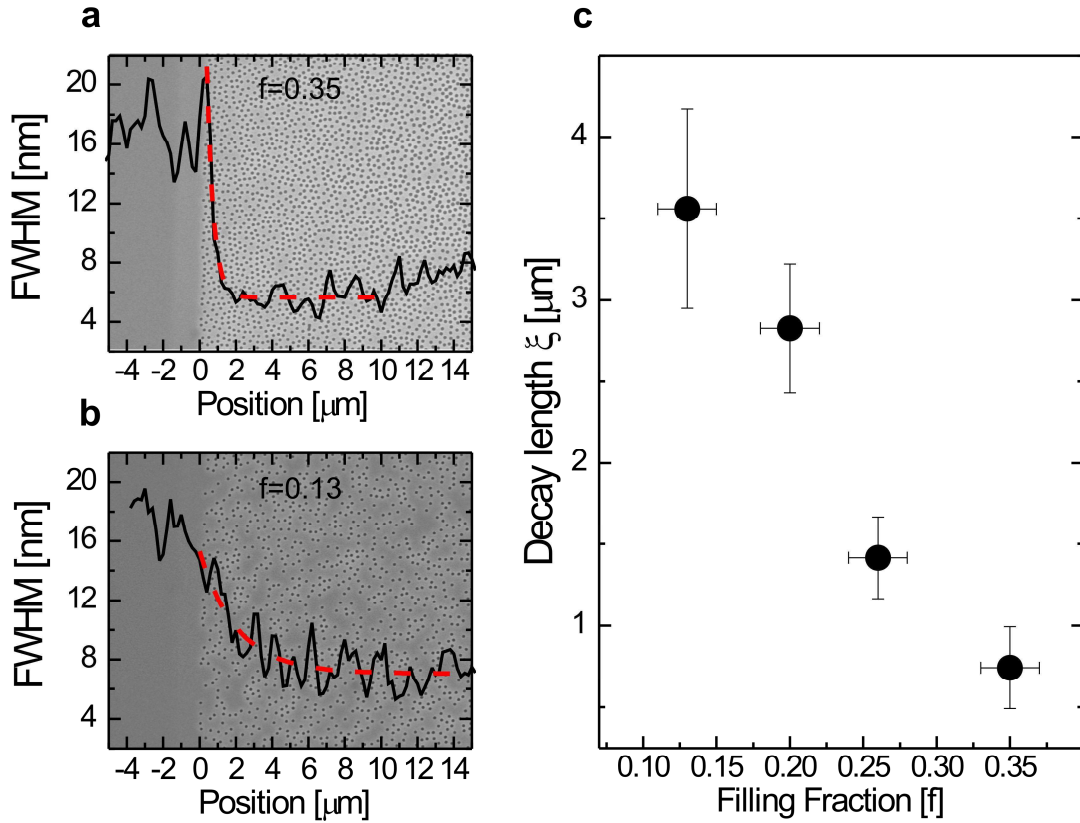
FIGURE 3: **Decay lengths of localized modes. a-b,** Average spectral width of near-field

frequency peaks as a function of the penetration depth inside the sample (black line). The

border of the samples is located at position x=0 μm. The red dotted line is an exponential fit

to the data. The FWHM of the average autocorrelation function was calculated within a

vertical strip parallel to the border of the sample. The size of the strip was 200 nm in the x-

direction and 9 μm in the y-direction and contains 45 near-field spectra. **c,** Average decay

lengths of photonic modes versus filling fraction, evaluated by fitting the decay of the average

spectral width with an exponential function (red dotted line in (**a**) and (**b**)). The errors are

evaluated by performing the above analysis along the four edges of each sample. The slight

increase of the FWHM in the bulk of the sample with f=0.35 is likely to be due to small

increase in the hole diameter caused by a proximity effect of the electron beam during the

writing stage. This effect is present at the center of the sample with high hole density and
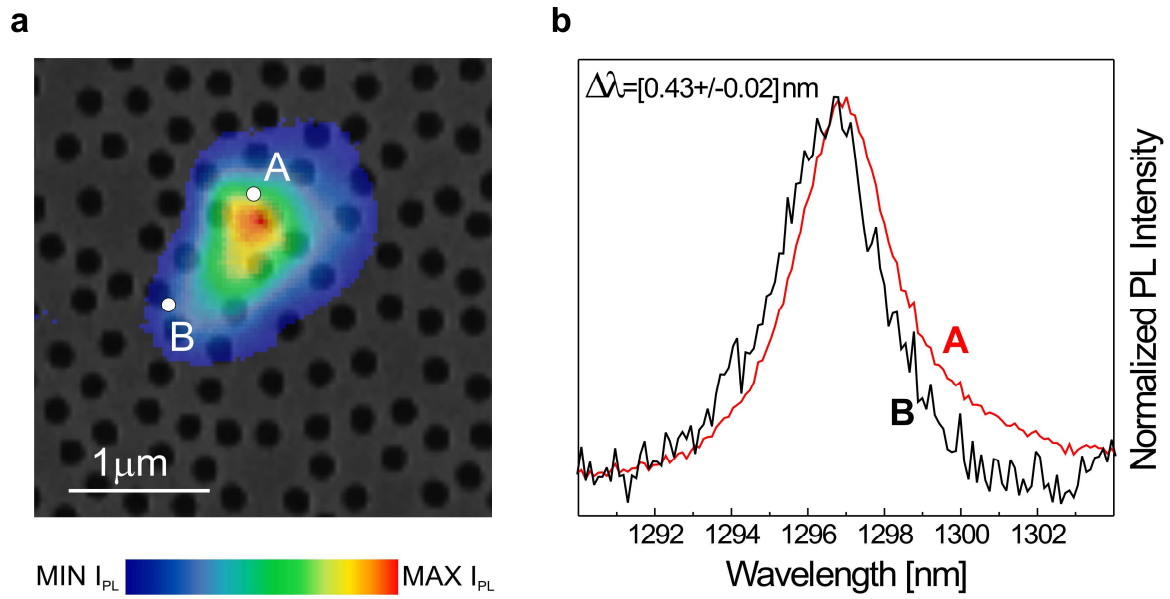
almost absent near the edges.

a

b

FIGURE 4: **Reversible spectral tuning of localized modes. a,** Maps of the PL intensity of the modes obtained by a Lorentzian fit of the local spectra. The color bar ranges from the maximum intensity to the minimum PL intensity. The spatial extension of the mode is consistent with the estimated decay length shown in Figure 3 (c). **b**, Normalized near-field spectra of the mode shown in panel (**a**), evaluated close to the maximum PL intensity (point A) and on a point showing low PL signal (point B). The mode shift is caused by the presence of the SNOM tip in the near-field of the mode, that induces a dielectric perturbation to the near field electric distribution of the mode. The observed maximum shift is 0.43 nm. The structural parameter of the sample are f=0.35 and h_d=220 nm.
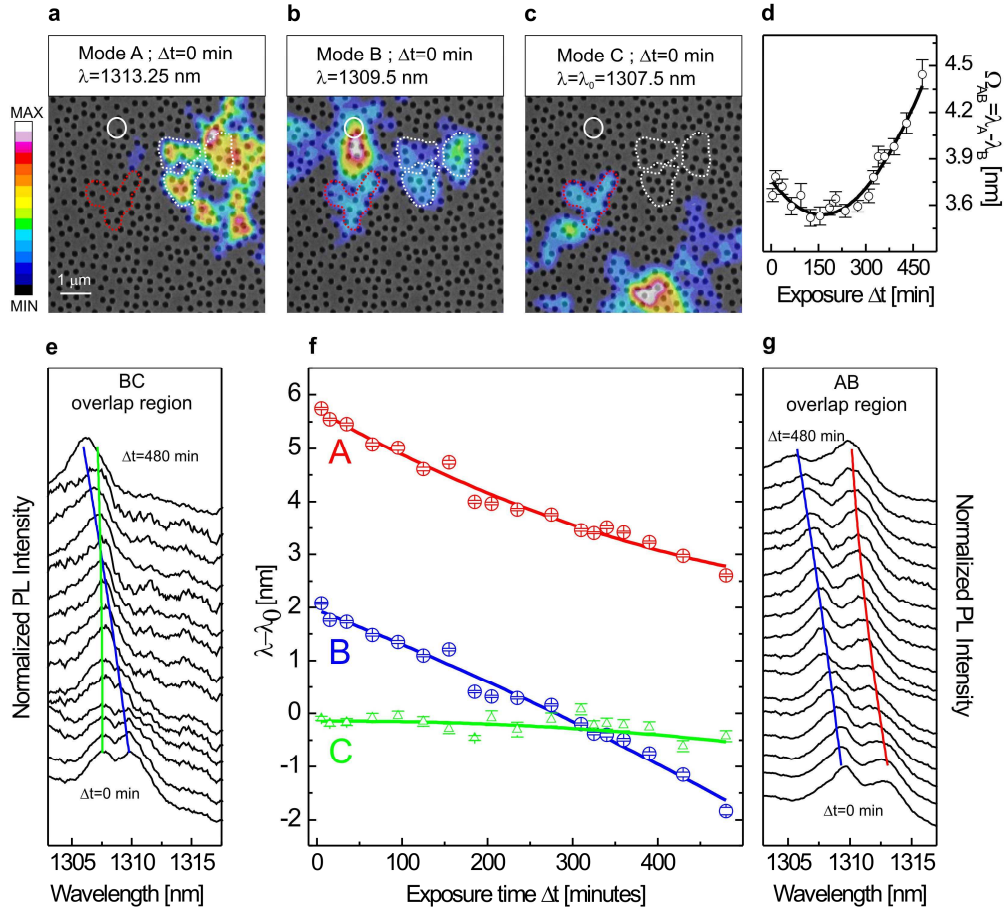
FIGURE 5: **Local engineering of localized modes. a-c,** Intensities of modes A, B and C

before starting the laser assisted local oxidation (Δt=0 min). The color bar of the images

ranges from MIN=0 to MAX=1 for mode B and mode C, and from MIN=0 to MAX=0.6 for

mode A. The white circle indicates the position of the SNOM tip during the photo-induced

oxidation of the GaAs membrane. The regions lying within the white (red) dotted lines identify

the spatial overlap between the modes A and B (B and C). Panel (**e**) and (**g**) show the

evolution of the normalized PL spectra mediated within the overlap regions (BC and AB,

respectively), as a function of the laser exposure time. The average intensity of the modes

within these regions is typically 10-15 times smaller than the average PL intensity of the

maxima of each mode. Panel (**f**) shows the evolution of the resonant wavelength of the three

modes evaluated in the overlap regions as a function of the exposure time Δt. The

separation between the resonant wavelengths of modes A and B ($\Omega_{AB}=\lambda_A-\lambda_B$) reaches a

minimum value of $\Omega^0_{AB}=2g=(3.55+/-0.25)$ nm at around Δt=170 min (panel (**d**)), while the

1

resonant wavelength of mode B crosses that of mode C at about Δt=310 min. The black solid line in panel (**d**) shows the fit of the experimental splitting with the expected trend for strong coupling.

Methods

Two-dimensional disordered photonic samples: structural parameters and growth process.

The disordered photonic system is realized on a GaAs planar dielectric waveguide 320 nm-thick suspended in air and clamped at its edges (Figure 1(a) and (b)), resulting in a square pad with lateral size L=25 μm. The planar waveguide is optically activated by the inclusion of three layers of high-density InAs quantum-dots (QDs), grown by molecular beam epitaxy. The QDs are buried in the middle plane of the slab, homogeneously distributed all over the sample and emit in a broad range of wavelengths, from 1.15 μm to 1.38 μm. The homogeneous and high density QDs distribution (about $10^3/\mu m^2$) guarantees that the bright spots in the intensity maps are in correspondence to underlying localized modes generated by multiple light scattering and are not caused by the fluctuation of the QD density. Electron-beam lithography, Reactive Ion Etching (RIE) and wet etching allowed to pattern the waveguide with a random distribution of circular holes. We realized samples with hole density ranging from f=0.13 to f=0.35 and hole diameter (h_d) ranging from h_d=180 nm to h_d= 250 nm. Deviations of the structural parameters from the nominal ones have been measured with a Scanning Electron Microscope and are within 5% for hole diameters and 10% for the filling fraction. In order to avoid merging between adjacent holes during the growth process (proximity effects), we imposed a minimum distance (1.3 hole diameter) between centers of nearest neighbouring holes.

Experimental setup: multidimensional near field imaging.

The experimental apparatus is a commercial SNOM (Twinsnom, Omicron). The SNOM is used in an illumination/collection geometry: QDs are excited through the SNOM tip with a 780 nm diode laser, and the PL signal is collected again through the same tip. The PL signal is dispersed in a spectrometer and detected by an InGaAs array. This allows to record point-by-point (with a combined spatial and spectral resolution of 200 nm and 0.5 nm, respectively) the local PL emission spectrum of the QDs. Spatial and spectral resolution can be improved up to 50 nm and 0.11 nm respectively, when necessary. These measurements provide therefore at the same time the spectral information, spatial distributions of the optical modes and structural information of the sample via the mechanical feedback signal of the SNOM. The large amount of data we are able to gather within a single experimental scan (more that $2 \cdot 10^5$ wavelength spectra, each one composed by 512 pixels), allows us to study the statistical properties of the near field intensity of photonic modes.

A crucial aspect in illumination/collection SNOM based setups is the fact that the PL intensity collected by the near-field tip results directly from (i) the excitation efficiency of the QDs, which is driven by the local density of optical states (LDOS) at the excitation wavelength (λ=780nm), (ii) QDs light emission efficiency, driven by the LDOS at the emission wavelength (ranging from λ=1150nm to λ=1380nm) and (iii) the collection efficiency of the near field probe. We thus expect the near field PL intensity measurements to indicate the location and extent of the photonic modes of the system, albeit not their exact intensity distribution.

To obtain intensity maps that reproduce in more detail the spatial profile of the modes, we used the well established tip induced perturbation technique [31,33-35]. The amount of the spectral shift $\Delta\lambda$ is directly proportional to the intensity of the local electric field and to the polarizability of the dielectric probe (SNOM tip), and inversely proportional to the modal volume V_{eff} of the localized mode. The polarizability of our tip, and therefore the measurement calibration of the modal volume from the spectral shift, has been determined by measuring the spectral shift in a photonic nanocavity with known V_{eff}. This allowed us to

reconstruct high fidelity intensity maps of localized modes and to give a careful estimation of the modal volume, $V_{eff} \sim 0.2 \mu m^3$, a value consistent with the measured decay length ($\xi \sim 0.8 \mu m$). The spatial distributions of mode A, mode B and mode C correspond to the amplitude of a Lorentzian fit of the mode PL spectra, as usually done for exploiting the tip induced perturbation technique.